Bacterial attachment to oxygen-functionalized graphenic surfaces

W. Pajerski[a,*], J. Duch[a], D. Ochonska[b], M. Golda-Cepa[a], M. Brzychczy-Wloch[b], A. Kotarba[a,*]

[a] *Faculty of Chemistry, Jagiellonian University in Krakow, Gronostajowa 2, 30-387 Krakow, Poland*
[b] *Department of Molecular Medical Microbiology, Chair of Microbiology, Faculty of Medicine, Jagiellonian University Medical College, Czysta 18, 31-121 Krakow, Poland*

ABSTRACT

In this work we have investigated the effect of oxygen plasma treatment of graphenic surfaces and the introduction of functional groups on changes in work function, wettability, surface free energy and bacterial adhesion. The plasma parameters were adjusted (generator power: < 60 W, exposure time: < 20 min) to limit the modifications to the surface without changing the bulk structure. The parent and modified graphenic surfaces were thoroughly characterized by μRaman spectroscopy, thermogravimetry, scanning electron microscopy, contact angle, X-ray photoelectron spectroscopy, work function and microbiological tests. It was found that even the short time of plasma modification results in a significant increase in work function, surface free energy and hydrophilicity. The changes in surface chemistry stimulate also substantial changes in bacterial adhesion. The strong relationship between work function and adhesion of bacteria was observed for all the investigated strains (*Staphylococcus epidermidis, Staphylococcus aureus, Pseudomonas aeruginosa, Escherichia coli*) whereas the bacterial colonization trend correlates with the bacterial zeta potential. The bacteria-graphenic surface interaction is discussed in terms of total interaction energy. The results point out the work function lowering of the graphenic biomaterial surface as an effective strategy for the infection risk limitation.

1. Introduction

The medical device industry has made enormous progress during the past decades, owing to the gained knowledge on the development of advanced materials technologies. Biomaterial devices and implants are investigated and used widely to improve patients' treatment, recovery, and quality of life [1–5]. Among a wide range of biomaterials (e.g. metal, ceramic, polymer, carbon-based) graphenic surfaces are of great interest due to their advantages such as good mechanical properties, large surface area, electrical and thermal conductivity, as well as tunable surface functionalities which play a pivotal role in regenerative medicine applications [1,6,7]. Graphene-based biomaterials are extensively investigated in recent years in the context of biological and medical applications such as, but not limited to stem cells differentiation, muscle tissue engineering, bone regeneration, drug delivery, gene therapy, photothermal therapy, dentistry, and bio-imaging [8–12]. Although graphene family materials have great potential in biomedical applications, there is a strong need to investigate their biological properties [9,13,14].

The major issue concerning the use of implantable materials is the infection risk and subsequent complications described as surgical-site infections (SSI) including implant and biomaterials-associated infections (BAI) [15–17]. According to the European Centre for Disease Prevention and Control, the SSI are the most common and in majority associated with additional treatment procedures, prolonged hospitalization, increased treatment costs, and higher mortality [18–20]. Depending on the surgical procedure type, the SSI can reach up to 9% yearly [18] and cause 8% of all deaths implicated by nosocomial infections [21].

Pathogens most frequently causing BAI include Gram-positive bacteria, like *Staphylococcus epidermidis, Staphylococcus aureus, Enterococcus* spp., *Streptococcus* spp., and Gram-negative bacteria, such as *Pseudomonas aeruginosa, Escherichia coli, Klebsiella* spp., *Enterobacter* spp. [18,22,23]. The prevention of bacteria-associated infections becomes more challenging due to their growing antibiotics resistance. Although there are several novel approaches to design surface with antibacterial properties including microbicidal surfaces coated with biocides [24–26], microbe-resistant surfaces with antiadhesive properties [27,28] and multifunctional materials combining both approaches [29,30], there is still a need to investigate mechanisms of interaction between bacteria and surfaces [14,31–33]. Although a lot of effort is put into the research on the BAI, there is still a lack of a universal solution to the problem, therefore the research on fundamental interactions may definitely contribute here. This is of particular

importance since the issue is unresolved so far and prevention guidelines are missing even in the newest SSI recommendations (Centers for Disease Control and Prevention 2017) [20].

The adhesion of microorganisms to the material surfaces is a complex biological process affected by many factors such as material composition, surface topography, electrostatic charge, surface free energy, wettability, and also the type of adjacent tissue [34–37]. Generally, biofilm formation consists of several subsequent steps including mass transport of bacteria to the surface, reversible cells' adsorption, changing to irreversible adhesion, microcolony formations leading to final biofilm production [34,36,38,39]. The phenomenon of initial step corresponding to early adhesion of bacteria to the surface is mediated by attractive and repulsive forces and explained based on the Derjaguin-Landau-Verwey-Overbeek (DLVO) theory. In order to obtain reliable and comprehensive picture the nature, range and energetics of dominating interactions at the biomaterial-bacteria interface have to be determined.

Several strategies to control the bacterial adhesion to biomaterials have been proposed so far [22,31,40–43]. One of the promising approaches is to tune the properties of biomaterials surfaces towards particular biological applications by chemical modifications [39]. In the case of carbon-based biomaterials, such modifications consist in the formation of specific surface moieties, e.g. functional groups [44] and/ or anchoring of biologically active molecules [45]. Among the wide range of surface functionalization methods, currently the most universal and efficient is oxygen plasma [46,47]. The most important practical advantage of low-pressure oxygen plasma, comparing with wet chemical methods, is definitely short functionalization time, precise control of the modification, and easy scale-up [48,49]. Moreover, cold plasma allows avoiding chemicals and producing waste, which are harmful to the environment. On the other hand, the careful plasma parameters optimization for each functionalization process and specific material is essential. Controlled introduction of oxygen surface species allows for tuning the surface properties such as electrodonor properties, wettability, polarity and as a consequence biocompatibility [50].

The aim of this study is to identify the key factors mediating the bacteria adhesion to functionalized graphenic surfaces. Precise control of surface oxygen concentration has been achieved by adjusting the oxygen plasma parameters. The investigations on biological response were focused on the initial step of bacteria colonization, which is crucial in infection and biofilm formation. In order to obtain the general model of bacteria adsorption, the investigations were carried out with the use of various pathogenic bacteria strains and a wide range of oxygen-modified graphenic surfaces. Such an approach allows for identifying key surface-related descriptors which have to be taken into account when designing novel implantable devices. The acquired knowledge is necessary for biocompatible surfaces with a low affinity towards bacteria.

2. Experimental

2.1. Samples preparation and modification

The conductive graphenic sheets supplied by Graphene Laboratories (Calverton NY, USA) were used in the study. The thickness of the material was 25 μm and a density of 2 $g \cdot cm^{-3}$. The samples used in all protocols and methods were in the form of squares (1 cm × 1 cm). In order to introduce oxygen species into the investigated graphenic sheets, the commercial cold plasma system (Femto-Diener Electronic GmbH, Nagold, Germany) was used. The experimental setup, plasma glow and idea of surface functionalization by oxygen are shown in Fig. 1.

The generator frequency was 40 kHz, the maximum temperature in the plasma chamber was kept below 30 °C. The plasma parameters (generator power, oxygen partial pressure, exposure time) were adjusted to achieve different modification levels in the electrodonor

properties of investigated graphene sheets, according to the parameters described elsewhere [51]. The modification of the carbon surface with oxygen plasma leads to the introduction of surface polar oxygen functional groups. The formed $C_{surf}^{\delta+} - O_{adatom}^{\delta-}$ dipoles result in the negative potential barrier and thus the work function, which is minimal energy required to electron escape from the surface to the vacuum level, increases. The changes in work function are directly related to the number of surface functional groups (Helmholtz relation) [52–54]. In Table 1 all the samples are listed together with the plasma parameters used for their modifications.

Directly after the modification, samples were investigated with the methods described in detail below. The applied protocols of the oxygen plasma surface modifications were found to be reproducible within the experimental error.

2.2. Methods

2.2.1. SEM observations

The investigated graphenic materials before and after microbiological investigations were characterized by the field-emission scanning electron microscope (FE-SEM, Hitachi S-4700). The samples with bacteria were fixed for the SEM observations following the protocol described elsewhere [55,56]. Briefly, samples were immersed in the fixative (3% buffered glutaraldehyde in Dulbecco's Phosphate Buffered Saline (DPBS, Lonza)) for 4 h, and then twice-washed with DPBS. Afterwards, dehydration was carried out with graded concentrations of water-ethanol solutions (50, 60, 70, 80, 90, 96, and 100%) for 10 min each. The prepared samples were attached to SEM holder using adhesive carbon tape and sputter-coated with a ~15 nm layer of gold (Quorum Q150T S).

2.2.2. μRaman spectroscopy

The μRaman measurements were carried out at room temperature using a Renishaw InVia spectrometer coupled to the confocal microscope. The 514.5 nm Argon ion laser with 1800 L/mm grating and 50× magnification lens was applied. Raman scattered light was collected in the characteristic for carbon materials range 1000–3500 cm^{-1}. For each sample, nine scans were accumulated to maximize signal to noise ratio.

2.2.3. X-ray photoelectron spectroscopy (XPS)

For determination of the surface elemental composition of investigated graphene samples before and after plasma modification, the XPS measurements were performed. The analysis was conducted in a UHV chamber (the vacuum level above 5×10^{-9} mbar). The device was equipped with a SESR4000 analyzer (Gammadata Scienta). The XPS spectra were recorded using the monochromatized Al-Kα source (1486.6 eV) working at 250 W with a pass energy of 100 eV for the narrow and survey scans. The resulting XPS spectra were calibrated for the C1s peak at 284 eV of the adventitious carbon and analyzed using Casa-XPS 2.3.15 software.

2.2.4. Water contact angle measurements and surface free energy (SFE) calculations

The contact angles were measured using a goniometer (Surftens Universal Instrument, OEG GmbH, Frankfurt (Oder), Germany) in order to determine changes in wettability and surface free energy (SFE) of the investigated graphene samples. The static contact angles for five 2.0 μL drops of two liquids (deionized water and diiodomethane) for each sample were measured and analyzed using windows image processing software (Surftens 4.3). The final contact angle value was an average of at least three independent experimental series for each sample (> 15 independent measurements for each liquid). The SFE was calculated using the Owens-Wendt method.
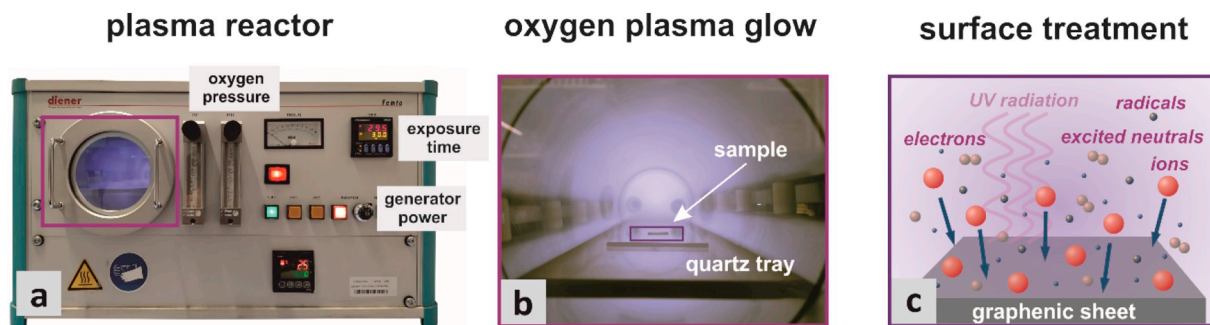
plasma reactor

oxygen plasma glow

surface treatment

Fig. 1. The plasma reactor used in the study (a), graphenic sample during oxygen functionalization in plasma chamber (b) and the schematic visualization of the surface treatment process (c).

Table 1
Samples used in the study and the parameters for their modifications.

Sample[a]	Generator power/W	Pressure/ mbar	Time/s	Work function/ eV	Surface concentration of functional groups[b]/N·cm^{-2}
$G_{4.4}$	–	–	–	4.4	–
$G_{4.5}$	2	0.14	2	4.5	$1.04 \cdot 10^{13}$
$G_{5.0}$	2	0.14	6	5.0	$4.85 \cdot 10^{13}$
$G_{5.4}$	20	0.20	2	5.4	$9.32 \cdot 10^{13}$
$G_{5.7}$	60	0.20	300	5.7	$1.23 \cdot 10^{14}$
$G_{6.0}$	60	0.50	1200	6.0	$1.62 \cdot 10^{14}$

[a] The number in sample label subscript indicates the work function value (see below).

[b] The surface coverage was evaluated following the Helmholtz formula [54]: $\Delta\Phi = Ne\mu/\varepsilon_0$ where $\Delta\Phi$ is the change in the work function [J], N is the number of adsorbed atoms per unit square, e is the elementary charge, μ is the dipole moment [C·m] and ε_0 is the vacuum permittivity.

2.2.5. Work function measurements

The work function values (Φ) of the investigated graphene samples were determined based on measurements of the contact potential difference (V_{CPD}) carried out by the Kelvin method with a KP6500 probe (McAllister Technical Services). As a reference electrode ($\Phi_{ref} \approx 4.3$ eV) the stainless-steel plate (diameter = 3 mm) was used. This area corresponds to the material surface covered by $\sim 10^6$ bacterial cells, thus providing good statistics for evaluation of bacterial adhesion. The gradient of the peak-to-peak versus backing potential was set to 0.1, the frequency at 114 Hz and the amplitude at 40 a.u. The work function values were calculated as an average of 60 independent measurements for each sample based on the relation: $\Phi_{sample} = \Phi_{ref} - eV_{CPD}$. The measurements were performed at ambient conditions (atmospheric pressure, room temperature).

2.3. Microbiological tests

2.3.1. Bacterial cultures preparation

The reference microorganisms used in the study were *Staphylococcus aureus* DSM 24167 (Deutsche Sammlung von Mikroorganismen und Zellkulturen), *Staphylococcus epidermidis* ATCC® 700296 (American Type Culture Collection), *Pseudomonas aeruginosa* ATCC® 27853 and *Escherichia coli* ATCC® 25922 (Fig. 2). The strains were incubated at 37 °C for 24 h in Bacto™ Tryptic Soy Broth (TSB, Becton Dickinson). Bacterial cells were harvested by centrifugation (13000 rpm, 5 min) and thrice-washed with DPBS. Then, the bacterial pellets were resuspended in DPBS and diluted to obtain bacterial suspensions of $\sim 3 \cdot 10^8$ CFU/mL (colony forming units) corresponding to 0.5 McFarland standard. The prepared bacterial suspensions were used in microbiological tests.

2.3.2. Bacterial zeta potential characterization

The bacterial zeta potential (0.5 McFarland in DPBS) was determined via electrophoretic light scattering in Zetasizer Nano ZS (Malvern Instruments, Malvern). All the measurements were performed in the same conditions, i.e. bacterial growth phase, pH and temperature.

The experiments were repeated at least three times to obtain the average value of the zeta-potential for each investigated bacterial strain.

2.3.3. Bacterial adhesion

The influence of oxygen plasma treatment on bacteria adhesion to tested graphenic surfaces was investigated using a fluorescent microscope (IX51 Olympus). The graphenic sheets samples (1 cm × 1 cm) were incubated immediately after the oxygen plasma modification with prepared bacterial suspensions (37 °C, 1 h) in the sterile 24-well plates. For each graphenic modification, the tests were performed in triplicates. To assure the reproducibility of the measurements three independent microbial tests were performed. Each time three graphenic sheets were modified and then the bacterial adhesion was evaluated. After the incubation, samples were gently washed in order to remove all non-attached microorganisms, fixed with 96% ethanol (POCH SA) and stained with the propidium iodide (PI, Sigma-Aldrich). At least 15 randomized images were taken for each sample and the area occupied by the bacteria was counted using Java open-source ImageJ software 1.51 k [57].

3. Results and discussion

Raman spectroscopy is the most suitable technique, commonly used for monitoring the structural changes of carbon-based materials upon functionalization [58]. Therefore, the effect of plasma treatment on the structure of investigated graphenic sheets was examined by μRaman spectroscopy (Fig. S1). The obtained Raman spectra for all graphenic materials exhibit characteristic for sp^2 carbon materials peaks at around 1580 cm^{-1} and 2725 cm^{-1}. The former band (G) comes from the first-order Raman scattering process and is related to in-phase vibration of the graphite lattice whereas the latter band (2D) arises from the second-order two-phonon process [59,60]. Only the application of prolonged plasma treatment and higher generator power results in slight changes on the graphenic surface (samples $G_{5.7}$ - $G_{6.0}$). Thus, the additional band (D) at 1350 cm^{-1}, indicated disorder degree in sp^2 carbon systems, can be noticed. Nevertheless, the low intensity of D band together with minor changes for the 2D band, demonstrated that upon applied plasma parameters the bulk structure of the investigated graphenic materials remained intact. Whereas the Raman spectroscopy is sensitive for carbon structural changes, it does not provide the information about the surface modifications.

In [51], the Laser Desorption/Ionization Mass Spectrometry was applied to monitor the effect of plasma modification of graphite, clearly
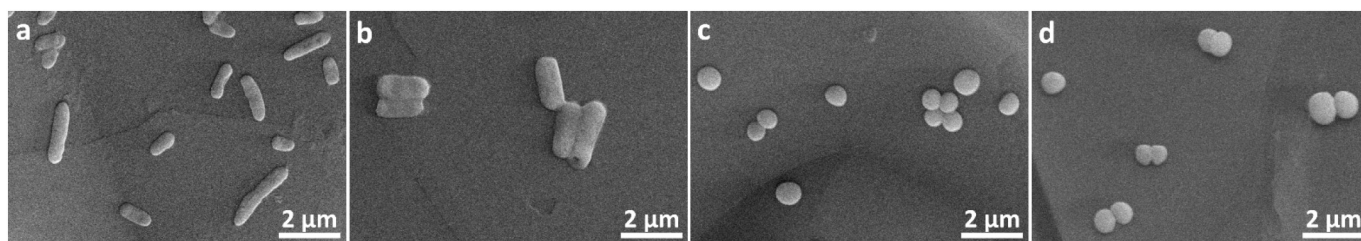
Fig. 2. Representative scanning electron microscopy images of bacteria cells, on the graphenic surfaces, selected for the study (a - *P. aeruginosa,* b - *E. coli,* c - *S. epidermidis,* d - *S. aureus)* showing differences in size and shape.
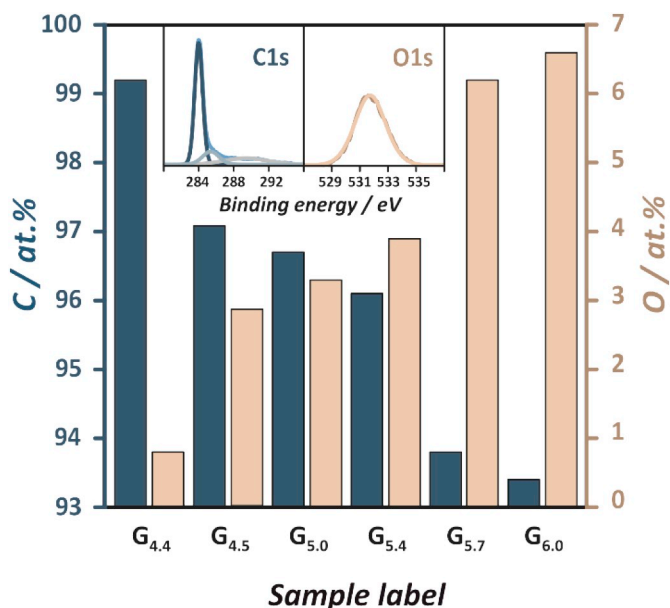

Fig. 3. XPS results showing the differences in surface composition (carbon and oxygen content) of the parent ($G_{4.4}$) and oxygen-plasma modified graphenic surfaces together with the representative narrow scans for the O1s and C1s peaks (insets) for sample $G_{5.4}$.

showing the incorporation of surface hydroxyl groups. Additionally, the thermogravimetric-differential thermal analysis (TG/DTA) of temperature-programmed oxidation for plasma-treated and untreated graphenic surfaces exhibits the same profiles (see Fig. S2), confirming that the bulk of the material remains unchanged upon interaction with plasma.

The chemical nature of the functional groups introduced via plasma treatment was further investigated by XPS. Since the graphenic material exhibit a flat surface, the XPS results can be reliably quantified. In Fig. 3 the XPS results for parent graphenic ($G_{4.4}$) and oxygen plasma-treated samples ($G_{4.5}$ - $G_{6.0}$) are summarized in terms of carbon and oxygen surface concentration changes. For the unmodified graphenic surfaces, the main constituting element (99.2% at.) was identified based on C1s peak at a binding energy of 284.0 eV (which can be attributed to sp^2 hybridized graphite-like carbon atoms) [61]. After exposure to plasma, a substantial increase in the O1s peak intensity at binding energy ~532 eV is observed for all of the investigated samples and the oxygen surface concentrations follow the trend 2.9, 3.3, 3.9, 6.2, 6.6% at. for $G_{4.5}$, $G_{5.0}$, $G_{5.4}$, $G_{5.7}$, $G_{6.0}$ samples, respectively. The deeper insight into the nature of oxygen-containing functional groups formed at graphenic surfaces was obtained by the deconvolution of XPS C1s peaks. For the oxygen-plasma treated samples, additional maxima were observed at ~285.2 eV and 290.0 eV, corresponding to $C-O$ and $O-C=O$, respectively [62]. These results are in line with the previously reported results for similar carbon surfaces [63,64].

The introduction of oxygen functional groups on the graphenic surfaces has a significant influence on the hydrophilic properties of the
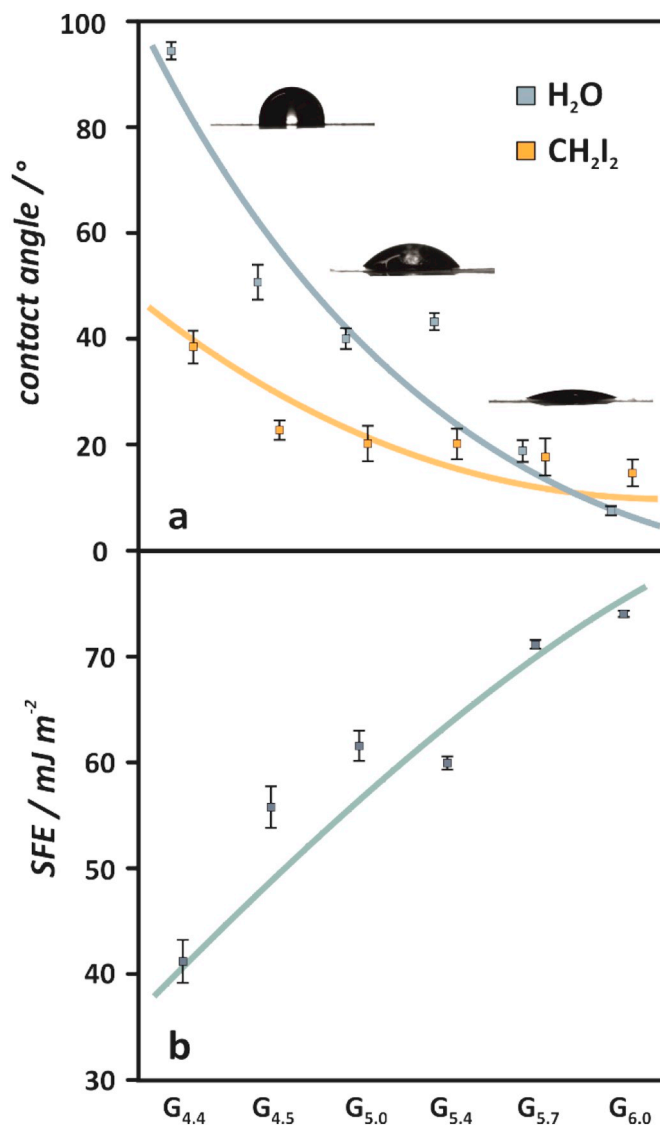

Fig. 4. Contact angle (a) and surface free energy values (b) for parent ($G_{4.4}$) and plasma-modified graphenic surfaces ($G_{4.5}$ - $G_{6.0}$).

material (Fig. 4). The water contact angle for unmodified surface ($G_{4.4}$) was found to be 94.5° ± 1.4° which classifies the material as a hydrophobic. Even a short exposition (several seconds) to oxygen plasma allows for turning the surfaces into hydrophilic. The values of the water contact angle (WCA) decreased to the range of 40.1°–50.8° for $G_{4.5}$ - $G_{5.4}$ samples. The plasma treatment with more severe conditions (power: 60 W) resulted in further reduction of WCA to 18.9° ± 2.1° ($G_{5.7}$) and eventually to 7.6° ± 0.9° ($G_{6.0}$). The decrease in contact angle was also observed for diiodomethane. As expected, for the non-polar solvent the changes were substantially smaller (Fig. 4), the

measured initial diiodomethane contact angle ($G_{4.4}$) was 38.5° ± 3.1° and after oxygen plasma treatment the value decreased to 17.7°–22.8° ($G_{4.5}$ - $G_{5.7}$) and reached 14.7° ± 2.5° for $G_{6.0}$ sample. As a result, the calculated total surface free energy γ_S (based on Owens-Wendt method) gradually increased for the oxygen plasma modified surfaces from 41.1 ± 2.0 mJ m^{-2} to 74.0 ± 0.3 mJ m^{-2} for the $G_{6.0}$ surface. The values of the components of surface free energy are summarized in Table 2 (S3). The polar component γ_S^P increased by 40.2 mJ m^{-2} whereas the dispersive component of surface free energy γ_S^D decreased by 7.3 mJ m^{-2}. Such a significant change of γ_S^P results from the successful introduction of polar oxygen functional groups at the graphenic surface upon plasma treatment [51]. It should be emphasized that, as discussed in previous studies [50,65–69], the changes in surface free energy strongly affect the interactions between the surface and living cells. Although a phenomenon of cell-surface adhesion is extensively investigated, presently there is no general theoretical framework for predicting the result of such interaction.

The obtained results clearly demonstrate that the graphenic material can be successfully modified with the use of plasma. Precisely adjusted treatment parameters allow limiting the changes to the topmost surface, without altering the materials bulk properties. The prepared series of graphenic sheets ($G_{4.4}$ - $G_{6.0}$) can be used as model surfaces for further studies on bacterial adhesion.

In order to determine the influence of surface modification via oxygen plasma on bacteria adhesion, the microbiological investigations were performed for several bacterial strains. The area of graphenic surfaces occupied by bacteria after 1 h incubation was estimated based on the analysis of fluorescence microscopic images. For a better insight into the nature of the observed phenomenon, more detailed SEM investigations of the bacteria adhered to graphenic surfaces were performed. Fig. 5a-b and c-d present the representative FM and SEM images of *S. epidermidis* and *E. coli*, respectively, adhered to $G_{4.4}$, $G_{5.4}$ and $G_{6.0}$ samples. The area occupied by bacteria increased with the extent of surface modification. In the case of the untreated sample ($G_{4.4}$) bacteria are located preferably in edges of the graphenic surfaces (Fig. 5 b1 and d1). Even a slight modification associated with an increase in $\Delta\Phi$ value (~0.1 eV) results in more homogenous bacterial adhesion.

In Fig. 6 the bacteria adhesion as a function of electrodonor properties (parametrized by Φ) of graphenic surfaces is presented. A similar correlation, the higher the work function the bigger the area occupied by bacteria, was previously reported for nanostructured titania implant surfaces of various topography colonized by *S. aureus* [53]. The same trend was observed for *S. aureus* adhesion on graphenic surfaces [51]. Here, the experiments are extended to other strains of Gram-positive (*S. aureus, S. epidermidis*) as well as Gram-negative (*P. aeruginosa, E. coli*) bacteria. The biggest difference in the area occupied is observed for *E. coli*, which exhibits the lowest zeta potential (net negative charge) in simulated body fluids (−23.0 mV), whereas for other investigated bacteria it ranges from −11.0 to −13.0 mV.

The interaction between the bacterial cell and the graphenic surface can be interpreted in terms of the Derjaguin-Landau-Verwey-Overbeek (DLVO) theory. Although this approach was developed for colloidal systems, it is successfully used in microbiology [70–74], also to describe the adhesion process of bacteria to solid surfaces [34,75,76]. The total free energy (V^{TOT}) is the sum of attractive London-van der Waals forces (V^{LW}) and electrostatic repulsive interactions (V^{EL}). Based on previous studies [34] (assuming that bacterial cells are homogenous spheres), the model for a sphere with the radii R interacting with a plate separated by the distance d can be approximated as:

$$V^{LW} = -\frac{AR}{6d} \tag{1}$$

$$V^{EL} = \pi\varepsilon \cdot R \left[2\zeta_B \psi_S \; ln\left(\frac{1 + exp^{-\kappa d}}{1 - exp^{-\kappa d}}\right) + (\zeta_B^2 + \psi_S^2) \; ln(1 - exp^{-2\kappa d}) \right] \tag{2}$$

$$V^{TOT} = V^{LW} + V^{EL} \tag{3}$$

where A is the Hamaker constant (10^{-20} J), ε is expressed as the product of the relative permittivity of the medium ε_r, which is 80 for DPBS at 20 °C, and the permittivity of a vacuum ε_0 ($8.854 \cdot 10^{-12}$ C^2/J·m); and ζ_B and ψ_S are the potentials of bacteria and surface, respectively, whereas κ is the inverse Debye-Hückel length (κ^{-1} = 0.76 nm for DPBS). The potential value for bacteria was represented by zeta potential whereas the surface potential can be approximated by the experimental value of contact potential difference.

The classic profile of interaction energy between bacteria and the surface exhibits a secondary minimum located at around 5 nm relates to reversible adsorption and primary energy minimum at ~1 nm which is related to irreversible adhesion. There is also an energetic barrier, which should be overcome by bacteria during the adhesion process. In Fig. 7a energy maxima of the interaction of *S. epidermidis* (−12 mV) with graphene surfaces $G_{4.4}$ - $G_{6.0}$ are shown. It can be noticed that the higher the Φ of the graphenic surface (higher concentration of surface oxygen groups, see Table 1), the higher the energetic barrier has to be overcome for bacteria to irreversibly adhere. Although the results are presented only for *S. epidermidis*, it is worth to mention that the same trends were observed for all the investigated bacteria strains. Passing from secondary, more distant, minimum to primary one is more energetically demanding for surfaces with higher Φ. The calculated activation barrier for adsorption changes from 10 to 90 kT (0.2–2.0 eV) corresponding well with similar values (50–150 kT) obtained for various bacteria interacting with flat inorganic surfaces, as described elsewhere [34,75,76]. It has to be emphasized that there is a strong correlation between the energetic barrier and the primary minimum depth. Such an energetic profile determines the overall interaction of bacteria with the graphenic surface. Once the energetic barrier is overcame, the adhesion becomes irreversible. For surfaces with a higher concentration of functional groups the bacteria adsorption is stronger and such surfaces are prone to infection and subsequent biofilm formation.

Since the interaction of bacteria with surfaces exhibits complex energetics there are no straightforward descriptors for evaluating the infection risk. Among several proposed approaches pointing out the importance of such parameters as wettability, SFE, surface charge, conductivity, roughness, recently the work function is proposed as a universal descriptor. The work function value can be expressed as a sum of Fermi energy (E_F) and surface potential (ψ_S): $\Phi = -E_F + e\psi_S$ [77]. It can be thus considered that upon bacteria approach the surface first the ψ_S is responsible for the interaction with the bacterial surface functional groups. Upon further approach the bacterial surface charge induces the image charge in the material. When negatively charged bacteria approach negatively charged surface, the so called image charge, with opposite sign appear in the contact place [78]. The efficiency of electron density dispersion over the conducting band is associated with the E_F. Such involvement of electrostatic interaction is especially important for the graphenic material which exhibits superior conductivity. The model of image charge/exchanging electrons between surface and bacteria cell is rationally explained. Indeed, the electrostatic model was applied for adhesion of bacteria (*S. epidermidis*) on the conducting surface and the charge of about 10^{-14}C per bacterium was exchanged during initial adhesion [79].

From the molecular point of view, the adhesion of bacteria to a flat surface is determined by the sum of interactions between functional groups located at external bacteria cell walls and the surface. In this study, the number of oxygen functional groups on graphenic surfaces was precisely controlled by plasma parameters. Whereas the bacterial colonized surfaces exhibited the same level of modification the used bacteria strains are characterized by the various chemical composition of cell walls. In Fig. 8 the number of –OH groups on graphenic surfaces per attached bacterial cells as a function of bacterial zeta potential is shown. The obtained experimental dependence clearly illustrates that
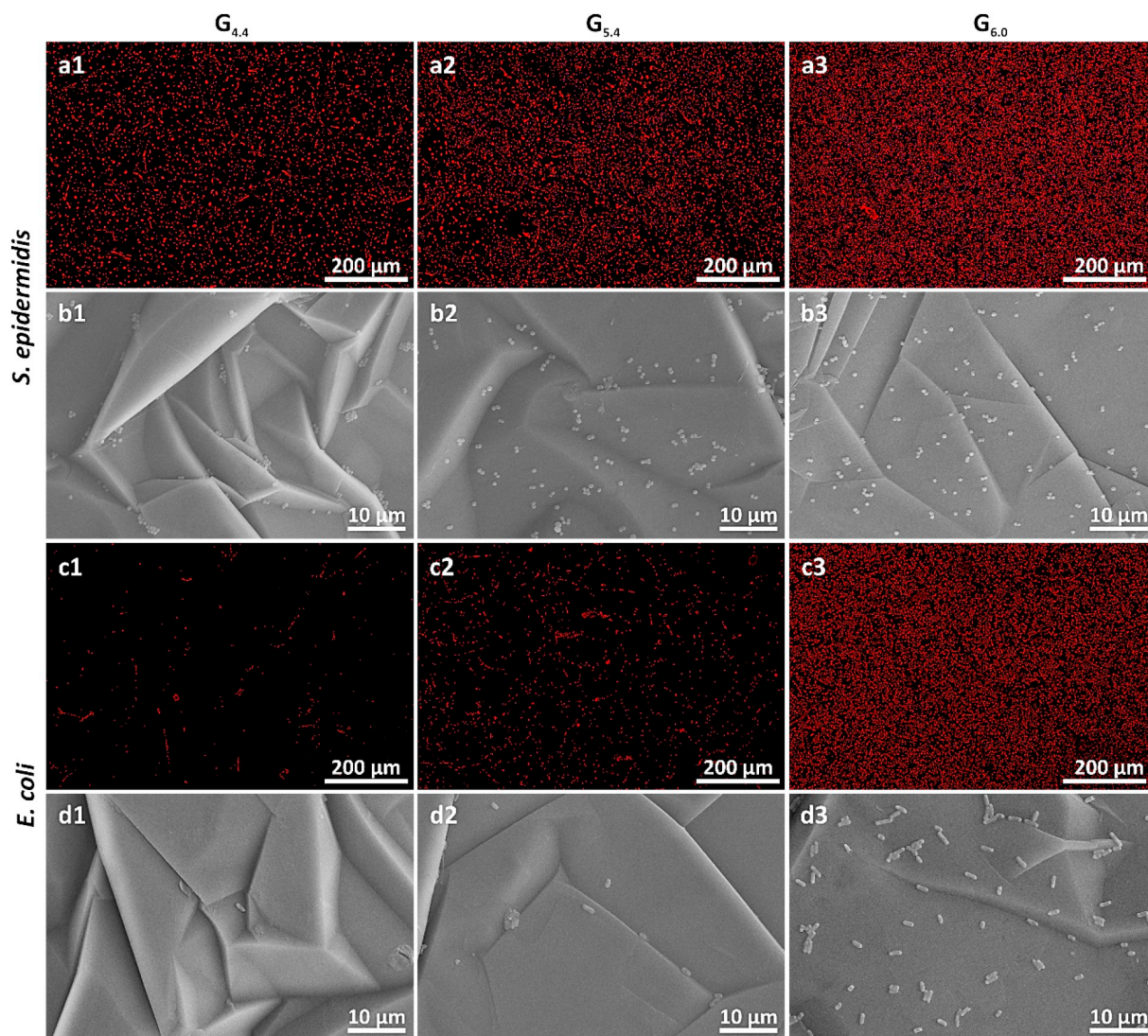
Fig. 5. Fluorescence microphotographs and scanning electron microscopy images of *S. epidermidis* (a1 - b3) and *E. coli* (c1 - d3) adhered to selected plasma-modified graphenic surfaces (G$_{4.4}$, G$_{5.4}$, G$_{6.0}$) after 1 h incubation. Such a short time of incubation was selected to probe the initial stage of the infection process. Experimental results for all the investigation samples and bacteria strains can be found in the Supporting Information (Fig. S4).

for lower zeta potential of bacteria, the higher the number of functional groups is needed for their irreversible adhesion. This can be explained in terms of the modification of electrodonor properties of the graphenic surfaces upon the introduction of oxygen. As previously shown, the surface oxygen groups lead to a substantial increase in the work function [52]. Furthermore, it was also reported that the adhesion of bacteria on carbon surfaces is dominated by the electrostatic interaction and the increase in Φ results in higher affinity of bacteria to the surface. It can be thus inferred that the higher surface coverage of graphenic surface with oxygen implies stimulation of bacteria adhesion. It should be emphasized that the oxygen functionalization of graphenic materials are considered as a beneficial procedure to improve surface wettability and biocompatibility [51,80]. In this context the obtained in this work results have important practical concerns, indicating the infection risk growth with the extent of oxygen plasma modification. It can be thus concluded that to minimize the bacteria adhesion the work function of graphenic surfaces should be lowered to limit the infection risk. Since the same trends were observed for all the investigated bacterial strains, the obtained results, indicating the strategy for biomaterials surface optimization, have a general practical meaning.

4. Conclusions

The effect of oxygen functional groups introduced to graphenic surfaces on bacterial adhesion was evaluated for a serious of micro-organisms: *Staphylococcus epidermidis, Staphylococcus aureus, Pseudomonas aeruginosa, Escherichia coli*. The modification of graphenic surfaces was accomplished by the application of low-temperature oxygen plasma treatment while adjusting the parameters for control surface modification (number of surface functional groups) without changing the bulk of the carbon materials. The introduction of surface dipoles (-OH$_{surf}$) results in substantial changes not only in surface chemistry of graphenic sheets but also in biological response (bacterial adhesion). It was found out that key factors of bacterial colonization are the electrodonor properties of the surface (work function) and the zeta potential of bacterial cells. The lowest colonization rate was observed for lower work function material (4.4 eV) and for bacteria with the lowest zeta potential (*E. coli*). The results were rationalized in terms of total interaction energy with the main contribution from electrostatic forces at the graphenic sheet-bacterial cell interface. It was concluded that the straightforward strategy for graphenic biomaterial surfaces protection against bacterial infection should involve lowering of the work function.
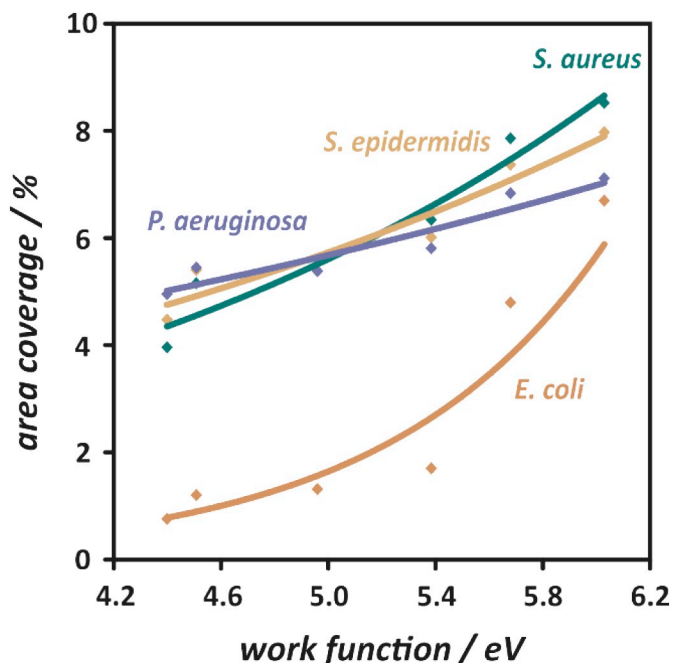
Fig. 6. The area occupied by *S. aureus*, *S. epidermidis*, *P. aeruginosa* and *E. coli* as a function of work function values for unmodified and plasma modified graphenic surfaces ($G_{4.4}$ - $G_{6.0}$).
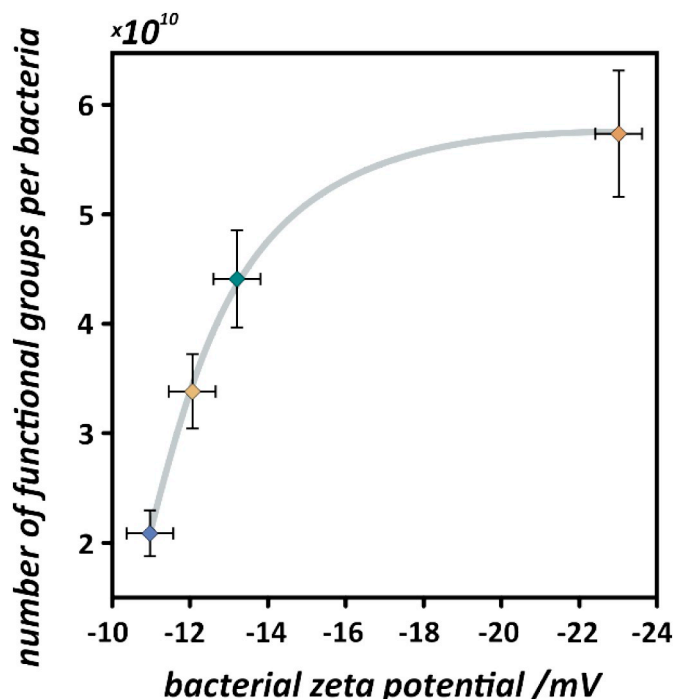

Fig. 8. The number of hydroxyl groups per bacteria attached to the surface with different zeta potential values ($R^2 > 0.99$).

Declaration of competing interest

The authors declare that they have no known competing financial interests or personal relationships that could have appeared to influence the work reported in this paper.

CRediT authorship contribution statement

W. Pajerski: Investigation, Visualization, Data curation, Validation, Writing - original draft. **J. Duch:** Investigation, Data curation, Visualization. **D. Ochonska:** Investigation. **M. Golda-Cepa:** Methodology, Validation, Project administration, Writing - review & editing. **M. Brzychczy-Wloch:** Validation, Resources, Writing - review & editing. **A. Kotarba:** Conceptualization, Supervision, Project administration, Funding acquisition, Resources, Writing - review & editing.

Acknowledgments

Appendix A. Supplementary data

Supplementary data to this article can be found online at https://doi.org/10.1016/j.msec.2020.110972.
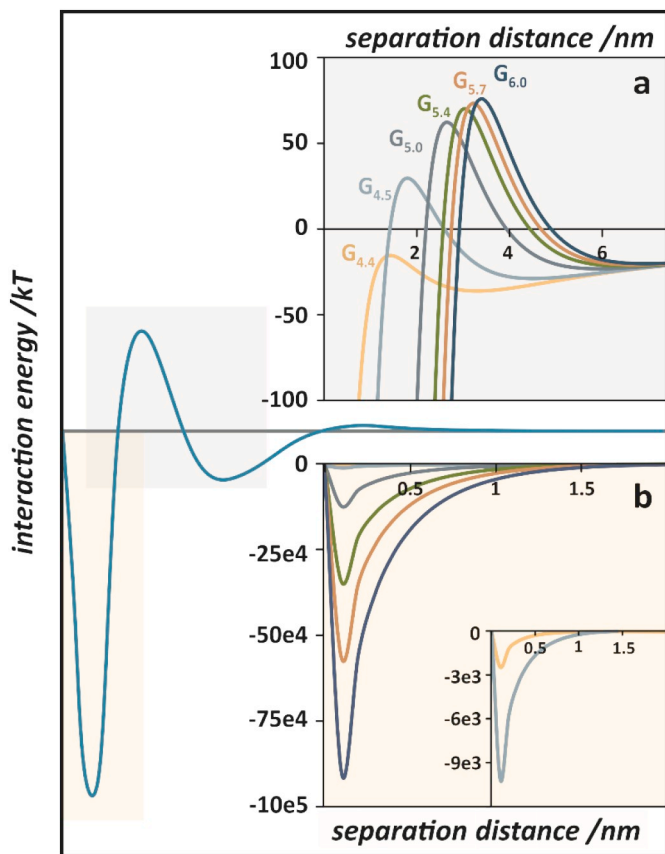

Fig. 7. Potential energy profiles for *S. epidermidis*-graphenic surfaces ($G_{4.4}$ - $G_{6.0}$) interactions calculated based on the DLVO theory. Energy maxima and energy minima are showed in the insets a and b, respectively.

References

[1] S. Kumar, M. Nehra, D. Kedia, N. Dilbaghi, K. Tankeshwar, K.H. Kim, Nanotechnology-based biomaterials for orthopaedic applications: recent advances and future prospects, Mater. Sci. Eng. C 106 (2020) 110154, , https://doi.org/10.1016/j.msec.2019.110154.

[2] Q. Zhang, W. Wu, C. Qian, W. Xiao, H. Zhu, J. Guo, Z. Meng, J. Zhu, Z. Ge, W. Cui, Advanced biomaterials for repairing and reconstruction of mandibular defects, Mater. Sci. Eng. C 103 (2019) 109858, , https://doi.org/10.1016/j.msec.2019.109858.

[3] Z.V. Parlak, S. Wein, R. Zybała, E. Tymicki, K. Kaszyca, S. Rütten, N. Labude, R. Telle, K. Schickle, S. Neuss, High-strength ceramics as innovative candidates for cardiovascular implants, J. Biomater. Appl. 34 (2019) 585–596, https://doi.org/10.1177/0885328219861602.

[4] C.R. Weinstein-Oppenheimer, D.I. Brown, R. Coloma, P. Morales, M. Reyna-Jeldes, M.J. Díaz, E. Sánchez, C.A. Acevedo, Design of a hybrid biomaterial for tissue engineering: biopolymer-scaffold integrated with an autologous hydrogel carrying mesenchymal stem-cells, Mater. Sci. Eng. C 79 (2017) 821–830, https://doi.org/10.1016/j.msec.2017.05.116.

[5] P.S. Kowalski, C. Bhattacharya, S. Afewerki, R. Langer, Smart biomaterials: recent advances and future directions, ACS Biomater. Sci. Eng. 4 (2018) 3809–3817, https://doi.org/10.1021/acsbiomaterials.8b00889.

[6] A. Navaei, K. Rahmani Eliato, R. Ros, R.Q. Migrino, B.C. Willis, M. Nikkhah, The influence of electrically conductive and non-conductive nanocomposite scaffolds on the maturation and excitability of engineered cardiac tissues, Biomater. Sci. 7 (2019) 585–595, https://doi.org/10.1039/c8bm01050a.

[7] S. Han, J. Sun, S. He, M. Tang, R. Chai, The application of graphene-based biomaterials in biomedicine, Am. J. Transl. Res. 11 (2019) 3246–3260.

[8] J. Jagiełło, M. Sekuła-Stryjewska, S. Noga, E. Adamczyk, M. Dźwigońska, M. Kurcz, K. Kurp, M. Winkowska-Struzik, E. Karnas, D. Boruczkowski, Z. Madeja, L. Lipińska, E.K. Zuba-Surma, Impact of graphene-based surfaces on the basic biological properties of human umbilical cord mesenchymal stem cells: implications for ex vivo cell expansion aimed at tissue repair, Int. J. Mol. Sci. 20 (2019), https://doi.org/10.3390/ijms20184561.

[9] Z.M. Wright, A.M. Arnold, B.D. Holt, K.E. Eckhart, S.A. Sydlik, Functional graphenic materials, graphene oxide, and graphene as scaffolds for bone regeneration, Regen. Eng. Transl. Med. 5 (2019) 190–209, https://doi.org/10.1007/s40883-018-0081-z.

[10] R. Dong, P.X. Ma, B. Guo, Conductive biomaterials for muscle tissue engineering, Biomaterials 229 (2020) 119584, , https://doi.org/10.1016/j.biomaterials.2019.119584.

[11] M. Tahriri, M. Del Monico, A. Moghanian, M. Tavakkoli Yaraki, R. Torres, A. Yadegari, L. Tayebi, Graphene and its derivatives: opportunities and challenges in dentistry, Mater. Sci. Eng. C 102 (2019) 171–185, https://doi.org/10.1016/j.msec.2019.04.051.

[12] C. Nie, L. Ma, S. Li, X. Fan, Y. Yang, C. Cheng, W. Zhao, C. Zhao, Recent progresses in graphene based bio-functional nanostructures for advanced biological and cellular interfaces, Nano Today 26 (2019) 57–97, https://doi.org/10.1016/j.nantod.2019.03.003.

[13] S. Goenka, V. Sant, S. Sant, Graphene-based nanomaterials for drug delivery and tissue engineering, J. Control. Release 173 (2014) 75–88, https://doi.org/10.1016/j.jconrel.2013.10.017.

[14] J. Ming, D. Sun, J. Wei, X. Chen, N. Zheng, Adhesion of bacteria to a graphene oxide film, ACS Appl. Bio Mater. 3 (2020) 704–712, https://doi.org/10.1021/acsabm.9b01028.

[15] M. Haque, M. Sartelli, J. McKimm, M.A. Bakar, Health care-associated infections – an overview, Infect. Drug Resist. 11 (2018) 2321–2333, https://doi.org/10.2147/IDR.S177247.

[16] H.J. Busscher, H.C. Van Der Mei, G. Subbiahdoss, P.C. Jutte, J.J.A.M. Van Den Dungen, S.A.J. Zaat, M.J. Schultz, D.W. Grainger, Biomaterial-associated infection: locating the finish line in the race for the surface, Sci. Transl. Med. 4 (2012), https://doi.org/10.1126/scitranslmed.3004528.

[17] Z. Khatoon, C.D. McTiernan, E.J. Suuronen, T.F. Mah, E.I. Alarcon, Bacterial biofilm formation on implantable devices and approaches to its treatment and prevention, Heliyon 4 (2018) e01067, , https://doi.org/10.1016/j.heliyon.2018.e01067.

[18] European Centre for Disease Prevention and Control, Healthcare-Associated Infections: Surgical Site Infections, Stockholm (2019).

[19] J.H. Kim, J. Kim, W.J. Lee, H. Seong, H. Choi, J.Y. Ahn, S.J. Jeong, N.S. Ku, T. Son, H. Il Kim, S.H. Han, J.Y. Choi, C.O. Kim, J.S. Yeom, W.J. Hyung, Y.G. Song, S.H. Noh, J.M. Kim, A.S. Levin, The incidence and risk factors for surgical site infection in older adults after gastric cancer surgery: a STROBE-compliant retrospective study, Medicine (Baltimore) 98 (2019) 1–6, https://doi.org/10.1097/MD.0000000000016739.

[20] S.I. Berriós-Torres, C.A. Umscheid, D.W. Bratzler, B. Leas, E.C. Stone, R.R. Kelz, C.E. Reinke, S. Morgan, J.S. Solomkin, J.E. Mazuski, E.P. Dellinger, K.M.F. Itani, E.F. Berbari, J. Segreti, J. Parvizi, J. Blanchard, G. Allen, J.A.J.W. Kluytmans, R. Donlan, W.P. Schecter, Centers for disease control and prevention guideline for the prevention of surgical site infection, JAMA Surg 152 (2017) (2017) 784–791, https://doi.org/10.1001/jamasurg.2017.0904.

[21] G. Collaborative, Determining the worldwide epidemiology of surgical site infections after gastrointestinal resection surgery: protocol for a multicentre, international, prospective cohort study (GlobalSurg 2), BMJ Open 7 (2017) 1–8, https://doi.org/10.1136/bmjopen-2016-012150.

[22] S.L. Percival, L. Suleman, C. Vuotto, G. Donelli, Healthcare-associated infections, medical devices and biofilms: risk, tolerance and control, J. Med. Microbiol. 64 (2015) 323–334, https://doi.org/10.1099/jmm.0.000032.

[23] D. Lebeaux, J.-M. Ghigo, C. Beloin, Biofilm-related infections: bridging the gap between clinical management and fundamental aspects of recalcitrance toward antibiotics, Microbiol. Mol. Biol. Rev. 78 (2014) 510–543, https://doi.org/10.1128/mmbr.00013-14.

[24] T.B. Donadt, R. Yang, Vapor-deposited biointerfaces and bacteria: an evolving conversation, ACS Biomater. Sci. Eng. 6 (2020) 182–197, https://doi.org/10.1021/acsbiomaterials.9b01496.

[25] M. Li, L. Li, K. Su, X. Liu, T. Zhang, Y. Liang, D. Jing, X. Yang, D. Zheng, Z. Cui, Z. Li, S. Zhu, K.W.K. Yeung, Y. Zheng, X. Wang, S. Wu, Highly effective and noninvasive near-infrared eradication of a Staphylococcus aureus biofilm on implants by a photoresponsive coating within 20 min, Adv. Sci. 6 (2019), https://doi.org/10.1002/advs.201900599.

[26] X. Xie, C. Mao, X. Liu, L. Tan, Z. Cui, X. Yang, S. Zhu, Z. Li, X. Yuan, Y. Zheng, K.W.K. Yeung, P.K. Chu, S. Wu, Tuning the Bandgap of photo-sensitive polydopamine/Ag3PO4/graphene oxide coating for rapid, noninvasive disinfection of implants, ACS Cent. Sci. 4 (2018) 724–738, https://doi.org/10.1021/acscentsci.8b00177.

[27] Y. Zhang, Y. Liu, B. Ren, D. Zhang, S. Xie, Y. Chang, J. Yang, J. Wu, L. Xu, J. Zheng, Fundamentals and applications of zwitterionic antifouling polymers, J. Phys. D. Appl. Phys. 52 (2019), https://doi.org/10.1088/1361-6463/ab2cbc.

[28] V.B. Damodaran, N.S. Murthy, Bio-inspired strategies for designing antifouling biomaterials, Biomater. Res. 20 (2016) 18, https://doi.org/10.1186/s40824-016-0064-4.

[29] X. Xie, C. Mao, X. Liu, Y. Zhang, Z. Cui, X. Yang, K.W.K. Yeung, H. Pan, P.K. Chu, S. Wu, Synergistic bacteria killing through photodynamic and physical actions of graphene oxide/Ag/collagen coating, ACS Appl. Mater. Interfaces 9 (2017) 26417–26428, https://doi.org/10.1021/acsami.7b06702.

[30] Z.K. Zander, M.L. Becker, Antimicrobial and antifouling strategies for polymeric medical devices, ACS Macro Lett. 7 (2018) 16–25, https://doi.org/10.1021/acsmacrolett.7b00879.

[31] S. Hogan, E. Kasotakis, S. Maher, B. Cavanagh, J.P. O'Gara, A. Pandit, T.E. Keyes, M. Devocelle, E. O'Neill, A novel medical device coating prevents Staphylococcus aureus biofilm formation on medical device surfaces, FEMS Microbiol. Lett. 366 (2019) 1–7, https://doi.org/10.1093/femsle/fnz107.

[32] C.R. Arciola, D. Campoccia, L. Montanaro, Implant infections: adhesion, biofilm formation and immune evasion, Nat. Rev. Microbiol. 16 (2018) 397–409, https://doi.org/10.1038/s41579-018-0019-y.

[33] C. Valotteau, N. Baccile, V. Humblot, S. Roelants, W. Soetaert, C.V. Stevens, Y.F. Dufrêne, Nanoscale antiadhesion properties of sophorolipid-coated surfaces against pathogenic bacteria, Nanoscale Horizons 4 (2019) 975–982, https://doi.org/10.1039/c9nh00006b.

[34] S. Wu, S. Altenried, A. Zogg, F. Zuber, K. Maniura-Weber, Q. Ren, Role of the surface nanoscale roughness of stainless steel on bacterial adhesion and micro-colony formation, ACS Omega 3 (2018) 6456–6464, https://doi.org/10.1021/acsomega.8b00769.

[35] Y. Chen, A.K. Harapanahalli, H.J. Busscher, W. Norde, H.C. van der Mei, Nanoscale cell wall deformation impacts long-range bacterial adhesion forces on surfaces, Appl. Environ. Microbiol. 80 (2014) 637–643, https://doi.org/10.1128/AEM.02745-13.

[36] J. Palmer, S. Flint, J. Brooks, Bacterial cell attachment, the beginning of a biofilm, J. Ind. Microbiol. Biotechnol. 34 (2007) 577–588, https://doi.org/10.1007/s10295-007-0234-4.

[37] S. Spriano, V. Sarath Chandra, A. Cochis, F. Uberti, L. Rimondini, E. Bertone, A. Vitale, C. Scolaro, M. Ferrari, F. Cirisano, G. Gautier di Confiengo, S. Ferraris, How do wettability, zeta potential and hydroxylation degree affect the biological response of biomaterials? Mater. Sci. Eng. C 74 (2017) 542–555, https://doi.org/10.1016/j.msec.2016.12.107.

[38] V. Carniello, B.W. Peterson, H.C. van der Mei, H.J. Busscher, Physico-chemistry from initial bacterial adhesion to surface-programmed biofilm growth, Adv. Colloid Interf. Sci. 261 (2018) 1–14, https://doi.org/10.1016/j.cis.2018.10.005.

[39] K. Hori, S. Matsumoto, Bacterial adhesion: from mechanism to control, Biochem. Eng. J. 48 (2010) 424–434, https://doi.org/10.1016/j.bej.2009.11.014.

[40] L.-C. Xu, Y. Wo, M.E. Meyerhoff, C.A. Siedlecki, Inhibition of bacterial adhesion and biofilm formation by dual functional textured and nitric oxide releasing surfaces, Acta Biomater. 51 (2017) 53–65, https://doi.org/10.1016/j.actbio.2017.01.030.

[41] I. Francolini, G. Donelli, Prevention and control of biofilm-based medical-device-related infections, FEMS Immunol. Med. Microbiol. 59 (2010) 227–238, https://doi.org/10.1111/j.1574-695X.2010.00665.x.

[42] M. Ramasamy, J. Lee, Recent nanotechnology approaches for prevention and treatment of biofilm-associated infections on medical devices, Biomed. Res. Int. 2016 (2016), https://doi.org/10.1155/2016/1851242.

[43] F.S. Lopes, J.R. Oliveira, J. Milani, L.D. Oliveira, J.P.B. Machado, V.J. Trava-Airoldi, A.O. Lobo, F.R. Marciano, Biomineralized diamond-like carbon films with incorporated titanium dioxide nanoparticles improved bioactivity properties and reduced biofilm formation, Mater. Sci. Eng. C 81 (2017) 373–379, https://doi.org/10.1016/j.msec.2017.07.043.

[44] M. Baraket, R. Stine, W.K. Lee, J.T. Robinson, C.R. Tamanaha, P.E. Sheehan, S.G. Walton, Aminated graphene for DNA attachment produced via plasma functionalization, Appl. Phys. Lett. 100 (2012) 233123, , https://doi.org/10.1063/1.4711771.

[45] M.G. Kim, J.Y. Park, W. Miao, J. Lee, Y.K. Oh, Polyaptamer DNA nanothread-anchored, reduced graphene oxide nanosheets for targeted delivery, Biomaterials 48 (2015) 129–136, https://doi.org/10.1016/j.biomaterials.2015.01.009.

[46] M. Gołda, M. Brzychczy-Włoch, M. Faryna, K. Engvall, A. Kotarba, Oxygen plasma functionalization of parylene C coating for implants surface: Nanotopography and active sites for drug anchoring, Mater. Sci. Eng. C 33 (2013) 4221–4227, https://doi.org/10.1016/j.msec.2013.06.014.

[47] E.C. Stancu, A.M. Stanciuc, S. Vizireanu, C. Luculescu, L. Moldovan, A. Achour, G. Dinescu, Plasma functionalization of carbon nanowalls and its effect on attachment of fibroblast-like cells, J. Phys. D. Appl. Phys. 47 (2014) 265203, , https://doi.org/10.1088/0022-3727/47/26/265203.

[48] C. Chen, B. Liang, A. Ogino, X. Wang, M. Nagatsu, Oxygen functionalization of multiwall carbon nanotubes by microwave-excited surface-wave plasma treatment,

J. Phys. Chem. C 113 (2009) 7659–7665, https://doi.org/10.1021/jp9012015.

[49] F. Khelifa, S. Ershov, Y. Habibi, R. Snyders, P. Dubois, Free-radical-induced grafting from plasma polymer surfaces, Chem. Rev. 116 (2016) 3975–4005, https://doi.org/10.1021/acs.chemrev.5b00634.

[50] M.M. Gentleman, E. Gentleman, The role of surface free energy in osteoblast-biomaterial interactions, Int. Mater. Rev. 59 (2014) 417–429, https://doi.org/10.1179/1743280414Y.0000000038.

[51] J. Duch, M. Golda-Cepa, A. Kotarba, Evaluating the effect of oxygen groups attached to the surface of graphenic sheets on bacteria adhesion: the role of the electronic factor, Appl. Surf. Sci. 463 (2019) 1134–1140, https://doi.org/10.1016/j.apsusc.2018.08.237.

[52] J. Duch, P. Kubisiak, K.H. Adolfsson, M. Hakkarainen, M. Golda-Cepa, A. Kotarba, Work function modifications of graphite surface via oxygen plasma treatment, Appl. Surf. Sci. 419 (2017) 439–446, https://doi.org/10.1016/j.apsusc.2017.05.007.

[53] M. Golda-Cepa, K. Syrek, M. Brzychczy-Wloch, G.D. Sulka, A. Kotarba, Primary role of electron work function for evaluation of nanostructured titania implant surface against bacterial infection, Mater. Sci. Eng. C. 66 (2016) 100–105, https://doi.org/10.1016/j.msec.2016.04.079.

[54] G.A. Somorjai, A.S. Mujumdar, Introduction to surface chemistry and catalysis, Dry. Technol. 13 (1995) 507–508, https://doi.org/10.1080/07373939508916972.

[55] W.F. Chissoe, E.L. Vezey, J.J. Skvarla, Hexamethyldisilazane as a drying agent for pollen scanning electron microscopy, Biotech. Histochem. 69 (1994) 192–198, https://doi.org/10.3109/10520299409106286.

[56] E.R. Fischer, B.T. Hansen, V. Nair, F.H. Hoyt, D.W. Dorward, Scanning electron microscopy, Curr. Protoc. Microbiol. (2012), https://doi.org/10.1002/9780471729259.mc02b02s25.

[57] K. Eliceiri, C.A. Schneider, W.S. Rasband, K.W. Eliceiri, NIH image to ImageJ: 25 years of image analysis HISTORICAL commentary NIH image to ImageJ: 25 years of image analysis, Nat. Methods 9 (2012) 671–675, https://doi.org/10.1038/nmeth.2089.

[58] A.C. Ferrari, J. Robertson, Interpretation of Raman spectra of disordered and amorphous carbon, Phys. Rev. B 61 (2000) 14095–14107, https://doi.org/10.1103/PhysRevB.61.14095.

[59] J.-P. Tessonnier, D. Rosenthal, T.W. Hansen, C. Hess, M.E. Schuster, R. Blume, F. Girgsdies, N. Pfänder, O. Timpe, D.S. Su, R. Schlögl, Analysis of the structure and chemical properties of some commercial carbon nanostructures, Carbon N. Y. 47 (2009) 1779–1798, https://doi.org/10.1016/j.carbon.2009.02.032.

[60] M.S. Dresselhaus, A. Jorio, M. Hofmann, G. Dresselhaus, R. Saito, Perspectives on carbon nanotubes and graphene Raman spectroscopy, Nano Lett. 10 (2010) 751–758, https://doi.org/10.1021/nl904286r.

[61] V. Datsyuk, M. Kalyva, K. Papagelis, J. Parthenios, D. Tasis, A. Siokou, I. Kallitsis, C. Galiotis, Chemical oxidation of multiwalled carbon nanotubes, Carbon N. Y. 46 (2008) 833–840, https://doi.org/10.1016/j.carbon.2008.02.012.

[62] T. Xu, J. Yang, J. Liu, Q. Fu, Surface modification of multi-walled carbon nanotubes by O2 plasma, Appl. Surf. Sci. 253 (2007) 8945–8951, https://doi.org/10.1016/j.apsusc.2007.05.028.

[63] K. Krishnamoorthy, M. Veerapandian, K. Yun, S.J. Kim, The chemical and structural analysis of graphene oxide with different degrees of oxidation, Carbon N. Y. 53 (2013) 38–49, https://doi.org/10.1016/j.carbon.2012.10.013.

[64] C. Vallés, J. David Núñez, A.M. Benito, W.K. Maser, Flexible conductive graphene paper obtained by direct and gentle annealing of graphene oxide paper, Carbon N. Y. 50 (2012) 835–844, https://doi.org/10.1016/j.carbon.2011.09.042.

[65] M. Nakamura, N. Hori, H. Ando, S. Namba, T. Toyama, N. Nishimiya, K. Yamashita, Surface free energy predominates in cell adhesion to hydroxyapatite through wettability, Mater. Sci. Eng. C. 62 (2016) 283–292, https://doi.org/10.1016/j.msec.2016.01.037.

[66] C.I. Pereni, Q. Zhao, Y. Liu, E. Abel, Surface free energy effect on bacterial retention, Colloids Surfaces B Biointerfaces 48 (2006) 143–147, https://doi.org/10.1016/j.colsurfb.2006.02.004.

[67] X. Zhang, Q. Zhang, T. Yan, Z. Jiang, X. Zhang, Y.Y. Zuo, Quantitatively predicting bacterial adhesion using surface free energy determined with a spectrophotometric method, Environ. Sci. Technol. 49 (2015) 6164–6171, https://doi.org/10.1021/es5050425.

[68] H. Koseki, A. Yonekura, T. Shida, I. Yoda, H. Horiuchi, Y. Morinaga, K. Yanagihara, H. Sakoda, M. Osaki, M. Tomita, Early staphylococcal biofilm formation on solid orthopaedic implant materials: in vitro study, PLoS One 9 (2014) 1–8, https://doi.org/10.1371/journal.pone.0107588.

[69] H. Ueno, M. Inoue, A. Okonogi, H. Kotera, T. Suzuki, Correlation between cells-on-chips materials and cell adhesion/proliferation focused on material's surface free energy, Colloids Surfaces A Physicochem. Eng. Asp. 565 (2019) 188–194, https://doi.org/10.1016/j.colsurfa.2018.12.059.

[70] W. Pajerski, D. Ochonska, M. Brzychczy-Wloch, P. Indyka, M. Jarosz, M. Golda-Cepa, Z. Sojka, A. Kotarba, Attachment efficiency of gold nanoparticles by gram-positive and gram-negative bacterial strains governed by surface charges, J. Nanopart. Res. 21 (2019), https://doi.org/10.1007/s11051-019-4617-z.

[71] M. Farahat, T. Hirajima, K. Sasaki, K. Doi, Adhesion of Escherichia coli onto quartz, hematite and corundum: extended DLVO theory and flotation behavior, Colloids Surf., B. 74 (2009) 140–149, https://doi.org/10.1016/j.colsurfb.2009.07.009.

[72] G. Hwang, I.S. Ahn, B.J. Mhin, J.Y. Kim, Adhesion of nano-sized particles to the surface of bacteria: mechanistic study with the extended DLVO theory, Colloids Surf., B. 97 (2012) 138–144, https://doi.org/10.1016/j.colsurfb.2012.04.031.

[73] X.M. Liu, G.P. Sheng, H.Q. Yu, DLVO approach to the flocculability of a photo-synthetic H 2-producing bacterium, Rhodopseudomonas acidophila, Environ. Sci. Technol. 41 (2007) 4620–4625, https://doi.org/10.1021/es070107n.

[74] A. Yoshihara, N. Nobuhira, H. Narahara, S. Toyoda, H. Tokumoto, Y. Konishi, T. Nomura, Estimation of the adhesive force distribution for the flagellar adhesion of Escherichia coli on a glass surface, Colloids Surfaces B Biointerfaces 131 (2015) 67–72, https://doi.org/10.1016/j.colsurfb.2015.04.038.

[75] S. Bayoudh, A. Othmane, L. Mora, H. Ben Ouada, Assessing bacterial adhesion using DLVO and XDLVO theories and the jet impingement technique, Colloids Surfaces B Biointerfaces. 73 (2009) 1–9, https://doi.org/10.1016/j.colsurfb.2009.04.030.

[76] A. Harimawan, S. Zhong, C.T. Lim, Y.P. Ting, Adhesion of B. subtilis spores and vegetative cells onto stainless steel - DLVO theories and AFM spectroscopy, J. Colloid Interface Sci. 405 (2013) 233–241, https://doi.org/10.1016/j.jcis.2013.05.031.

[77] A. Oprea, N. Bârsan, U. Weimar, Work function changes in gas sensitive materials: fundamentals and applications, Sensors Actuators B Chem. 142 (2009) 470–493, https://doi.org/10.1016/j.snb.2009.06.043.

[78] L. Mei, H.C. Van Der Mei, Y. Ren, W. Norde, H.J. Busscher, Poisson analysis of streptococcal bond strengthening on stainless steel with and without a salivary conditioning film, Langmuir 25 (2009) 6227–6231, https://doi.org/10.1021/la9000494.

[79] A.T. Poortinga, R. Bos, H.J. Busscher, Measurement of charge transfer during bacterial adhesion to an indium tin oxide surface in a parallel plate flow chamber, J. Microbiol. Methods 38 (1999) 183–189, https://doi.org/10.1016/S0167-7012(99)00100-1.

[80] L. Yan, M. Lin, C. Zeng, Z. Chen, S. Zhang, X. Zhao, A. Wu, Y. Wang, L. Dai, J. Qu, M. Guo, Y. Liu, Electroactive and biocompatible hydroxyl- functionalized graphene by ball milling, J. Mater. Chem. 22 (2012) 8367, https://doi.org/10.1039/c2jm30961k.